MOLECULAR PHYSICS, 1980, VOL. 40, No. 6, 1357–1377

The analysis of molecular dynamics with a range of microwave/far infrared spectra

by C. J. REID and M. W. EVANS
Chemistry Department, University College of Wales,
Aberystwyth SY23 1NE, Wales

(*Received* 4 *December* 1979 ; *revision received* 8 *February* 1980)

A Mori approximant for zero-THz absorptions of dipolar solutes is tested thoroughly with several examples. A number of points emerge from the data correlation.

(i) It is advantageous to analyse the complicated theoretical expressions before attempting a best fit analysis. Curve matching should be performed in both time and frequency domains.

(ii) The theory is sufficient at short and long times but the evolution at intermediate times is not followed satisfactorily. This shows up clearly in the 10–50 cm^{-1} region of the far infrared.

(iii) The far infrared peak frequency is not related straightforwardly to the theoretical mean square torque, but via parameters grouped about 2·6 for the two dozen or so systems studied.

(iv) The measured Debye relaxation times (this work) are reproduced theoretically from the far infrared to within about 30 per cent of their values for most solutes, but progressively poorer results are obtained as the molecular size increases, and as the molecules become more anisotropic.

(v) It is essential to consider in detail the effects of collision-induced absorptions and other mechanisms of permanent dipole enhancement. The failure of the Gordon sum rule cannot be attributed solely to this cause and rototranslational interaction probably plays a significant role.

1. INTRODUCTION

In previous publications [1–3] we have used a three variable Mori continued fraction approximant for the orientational autocorrelation function, to describe the spectral features of dipolar liquids and liquid mixtures over the zero to the THz frequency range and hence emphasize the causal link between classical dielectric and far infrared (F.I.R.) behaviour. This approach, referred to as method (i), is a development of a method first used by Nee and Zwanzig [4], and includes memory and inertial effects which are needed to reproduce even the most basic features of absorption spectra in the F.I.R.—the Poley absorption. In the short-time domain [2, 5], the formalism has clear advantages over earlier models which correspond to lower order approximants in the Mori formalism.

More recently we have been developing an analytical model [6–9] whereby this formalism is applied to the angular velocity autocorrelation function of a dipole vector which is then constrained to move in a plane in order to calculate

0026-8976/80/4006 1357 $02·00

the orientational autocorrelation function analytically [10]. This approach, method (ii), has the advantage that it can be given a mechanical meaning in terms of the planar itinerant oscillator model of Coffey *et al.* [11] (henceforth referred to as the Mori/I.O. model). Methods (i) and (ii) both have advantages and disadvantages [3], but recently Reid [12] has combined the statistical and physical interpretations of method (ii) to derive an approximate relation between the product $I_r\bar{\nu}_{max}^2$ (where $\bar{\nu}_{max}$ is the absorption peak wave number and I_r the reduced inertia of the polar species) and the mean square torque. The further reduction [8, 9] of this torque into a product of solute and solvent contribution allows a prediction (for dilute systems of common solvent and temperature) of the solute librational absorption centre ($\bar{\nu}_{max}$) from the solute volume of rotation. This relation, which appears to be well verified for a series of rigid solutes dissolved in decalin at 293 K [9], may prove useful in the investigation of mode–mode couplings, association and H-bonding effects in solutions, and as evidence for unresolved proper modes in, for example, tetrahydrofuran (pseudo-rotation) [12].

The aim of this paper is to evaluate method (ii) in greater depth by testing whether the Mori/I.O. model can reproduce adequately, the spectral profiles of suitable liquid systems (of small dipolar molecules) which, presentable either as absorption $\alpha(\bar{\nu})$ or as dielectric loss $\epsilon''(\omega)=\omega^{-1}\alpha(\omega)n(\omega)c$, extend over the range 10^9 to 10^{13} Hz.

In order to do this it is advantageous to compare theoretical and experimental curves in the short-time region [12]. This is because firstly, the approximation of a non-dispersive internal field and of single molecule autocorrelation are more acceptable in this region, and secondly, behaviour at short times provides a critical test of any model of the liquid state [5]. At long times the orientational correlation function very often appears to be a pure experimental decay, too easily reproduced by a wide variety of theoretical models. The Mori/I.O. equation for the rotational-velocity autocorrelation function [15] is fitted in this paper to the transformed spectra of a number of dilute solutions of dipolar molecules in decalin at 293 K. A comparison is then possible in terms of three best-fit parameters, $K_0(0)$, $K_1(0)$ and γ which are defined in the Appendix. In particular, we test the extent to which the orientational autocorrelation function determined from the high frequency (20–200 cm^{-1}) data given by a single interferometric experiment, can be extrapolated through the 0 to 20 cm^{-1} region and so predict dielectric behaviour. Such predictions are confirmed by spot-frequency measurements performed in the 4 to 70 GHz region and further indicate the basic validity of the Mori/I.O. approach.

2. Theoretical

The Mori/I.O. model, so called to emphasize the dual interpretation that this model affords and also to distinguish this three-variable formalism from a generalized version of the I.O. model [7] which we have studied in connection with viscous and glassy media [14], has been discussed in the literature from several theoretical points of view [6–12]. To aid in our discussion, the main features of this theory together with the relations required for the present application are grouped in an appendix. Of primary importance is equation (A 11) for the rotational velocity autocorrelation function $C_\mu(t)$ which is to be

spectrum [15]

$$C_{\dot{\mu}}(t)_{exp}=\frac{6kT\epsilon_0 c}{N\mu^2}\left[\frac{9n}{(n^2+2)^2}\right]\int_0^\infty \alpha(\omega)\cos(\omega t)\,d\omega, \qquad (1)$$

where ϵ_0 is the vacuum permittivity and n the F.I.R. refractive index.

Several basic points need to be considered in such a comparison. Firstly the analytic equation (A 11) derived [10] for planar reorientation of a dipole in a disc of inertia I is assumed [8] to be valid for real systems when the reduced inertia I_r [13] is used as the appropriate measure of inertia. Secondly the proportionality factor in (1) may not be entirely adequate in view of the uncertainty of internal field effects so that we prefer to match the theoretical and experimental time curves only in profile. As regards the actual fitting procedure, the time unit is chosen to be $(I_r/kT)^{1/2}$. This removes the factor kT/I_r from (A 7) (and hence (A 11)) and also factors of about 10^{12} from the coefficients. Iteration is best performed on the initially guessed values of α_1, α_2 and β rather than on $\bar{K}_0$, $\bar{K}_1$ and $\bar{\gamma}$ (the bars denoting normalized units) as it is easier to determine the latter from the former using relations (A 6) than it is to do the reverse using Cardan's formulae [6]. The particular influence on the iteration procedure, of α_1, α_2 and β can also be more easily assessed. Thus β, appearing in the dominant $\cos(\beta\bar{t})$ term, determines the position of the minimum of $C_{\dot{\mu}}(\bar{t})$ while α_1 in the damping factor $\exp(-\alpha_1\bar{t})$ determines the depth of the minimum. The parameter α_2 is found only to significantly affect the shape of $C_{\dot{\mu}}(\bar{t})$ if its value is comparable with or smaller than the value of β, otherwise it becomes redundant. This makes it necessary to consider both time and frequency domain data in the determination of optimal values for K_0, K_1 and γ although as will be shown later, the imperfect spectral profiles generated by the Mori/I.O. model complicates this process. For the present it is convenient (and suitably accurate) to summarize our attempts at spectral curve matching by stating that the value of α_2 should be chosen to equal the best fit value of β. Using this empirical result as an assumption valid for all the systems studied here, best-fit values of K_0, K_1 and γ can now be obtained from the single operation of curve matching in the short-time domain. These results are summarized in table 1 and the adequacy of the fits shown in figure 1. The systems studied were chosen for the accuracy for which the experimental $C_{\dot{\mu}}(t)_{exp}$ curves may be obtained. Decalin (70 per cent cis isomer) was chosen as the common solvent as it has a very low cross-sectional absorption in the far infrared. As all solution spectra are corrected by algebraic subtraction of the solvent absorption, the smaller the latter the less important is any error incurred in this correction. The solutes were chosen for their possessing

(i) rigidity, the dipole vector remaining fixed in the molecular frame allowing I_r to be calculated ;
(ii) a well-defined librational bandshape undistorted by (or corrected for) higher frequency proper modes ;
(iii) a reasonably intense absorption to minimize experimental uncertainties (such as solvent correction) and the effects of collision induced absorption ;
(iv) freedom from reactivity, H-bonding and other forms of association (aniline and acetone are included to show these effects).

Table 1. Best-fit data for decalin systems at 293 K.

Solute (10 per cent v/v)	$(I_r/kT)^{1/2}$/ps	α_1	β	$\bar{K}_0$ (reduced time units)	$\bar{K}_1$	$\bar{\gamma}$	$K_0/(\text{ps})^{-2}$	$\tilde{\nu}_{max}/\text{cm}^{-1}$	K_0/ω_{max}
(1) Pyridine	0·48	3·1	8·0	41·5	81·8	14·2	180	45	2·5
(2) Fluorobenzene	0·69	3·7	9·7	61	118	17·1	128	39	2·37
(3) Chlorobenzene	0·85	3·6	10·8	77·7	130	18	108	34	2·6
	0·97	4·1	12·8	110	176	21	117		2·84
(4) Bromobenzene	1·04	6·0	11·5	82	224	23·5	76	24	(3·7)
	1·27	6·7	15·2	147	333	28·6	91		(4·4)
(5) Nitrobenzene	0·98	5·6	15	147	277	26·2	153	39	2·8
	1·15	6·7	18	211	398	31·4	159		2·94
(6) Benzonitrile	0·87	4·6	14·2	135	218	23·4	178	47	2·26
(7) α-Picoline	0·55	2·75	10	69·4	93	15·5	230	60	1·8
(8) Toluene	0·69	2·75	11·8	100	112	17·3	210	60	1·64
(9) Pentafluorobenzene	1·04	5	14	129	232	24	119	30	3·7
(10) Chloronaphthalene	1·0	4	14·3	141	193	22·3	136	47	1·73
(11) Aniline	0·69	2·3	12·3 ($\alpha_2=7$)	94·5	94·3	11·6	198	64	(1·35)
(12) Bromonaphthalene	1·13	4·8	14·9	149	239	24·5	117	38	2·27
	1·32	5·5	17·5	207	322	28·5	118·6		2·3
(13) Furan	0·38	2·5	7·2	34·3	60	12·2	237	51	2·56
(14) Tetrahydropyran	0·53	3·5	9·1	53·7	105	16·1	191	41	3·2
(15) Thiazole	0·45	2·7	7·4	35·9	66	12·8	177	45	2·46
(16) Chlorocyclohexane	0·78	3·0	8·8	51·4	87·8	14·8	84·5	32	2·32
(17) *t*-Butylchloride	0·59	3·2	6·5	26·4	67·6	12·9	76	24	3·7
(18) Chloroform	0·55	3·6	7·0 ($\alpha_2=8$)	32·6	27	15·2	108	30	3·36
(19) 2-Chloro 2-nitropropane	0·7	3·6	8·8	49·7	104	16	101·4	33	2·6
(20) CH_2Cl_2	0·24	1·6	4·8 ($\alpha_2=3·5$)	13·4	23·4	6·7	232	52	2·6
(21) Acetone	0·53	2·5	7·2	34·3	60	12·2	122	53	(1·2)
(22) Methyliodide	0·37	2·3	7·3	35·9	56·2	11·9	262	60	2·05
(23) CH_2Br_2	0·27	1·45	5 ($\alpha_2=4$)	15·7	23	6·9	215	55	2·0

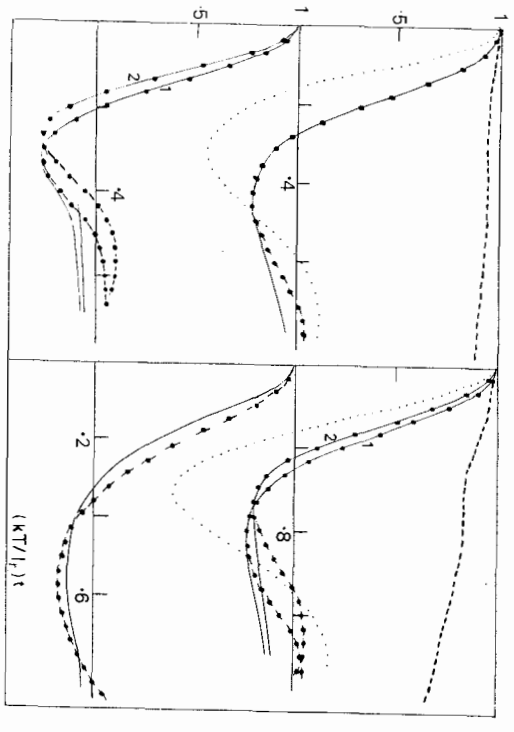

(c) (d)

Figure 1. Time curve matching exercises for selected solutes in decalin solution (293 K) illustrating some points of interpretation. (*a*) Pyridine–decalin : ———, experimental rotational velocity autocorrelation function ; –●– –●– –●–, best fit to above ; ·····, total torque autocorrelation function (analytic) ; – – – – –, orientational autocorrelation function (analytic). (*b*) CH_2Cl_2–decalin. As for figure 2 (*a*) with the experimental curve obtained from : (1) the spectral mean of seven experiments ; (2) an extremum. (*c*) Chlorobenzene–decalin as figure 2 (*a*). I_r values chosen about : (1) centre of mass axes ; (2) torque determined axes. (*d*) Chloroform–decalin as figure 2 (*a*).

We emphasize that the form of $C_\mu(t)_{exp}$ is adequately determined from the data (over the 20–200 cm^{-1} range) provided by a single far infrared interferometric experiment. For the numerical transformation the bandshape is extrapolated (without consideration of microwave data) down to zero frequency, reasonable extremes of extrapolation giving negligible error. The best fit parameters so obtained may then be used to generate the forms of other correlation functions including that of orientation (equation (A 7)) which underlies the microwave behaviour below about 20 cm^{-1}. This allows a prediction of dielectric behaviour described principally by the microscopic relaxation time $\tau_{Nori}=(I_r/kt)\cdot\gamma K_0/K_1$ or given spectrally (as loss $\epsilon''(\omega)=n(\omega)\alpha(\omega)c/\omega$ by (A 13).

The trends in parameters γ, K_0 and K_1 are analysed both in terms of statistical concepts (the mean square torque and the causal linking of loss and absorption peaks) and through the concept of itinerant oscillation.

3. Experimental

Spectra were taken with a phase modulated Grubb–Parsons/N.P.L. interferometer using standard techniques of Fourier transform spectroscopy [16] and some have been presented before [9]. The data acquisition was spread over a period of twelve months in order to minimize instrumental uncertainty. Microwave attenuation measurements employed standard waveguides for 35 and 70 GHz points and the sweep frequency method of Price [17] for the range from 4 to 18 GHz. The numerical transformations were performed using a Simpson's rule algorithm.

4. Results and discussion

The best fit results are summarized in table 1 and provide adequate descriptions of the experimental rotational velocity correlation functions exemplified in figure 1. Here the experimental curves (full lines) decay initially as cosines and are followed by the Mori/I.O. fittings until they deviate beyond the first half period of the oscillation. Three further points on the curve matching analyses are exemplified in the figure and will be considered in turn.

We have already pointed out [8, 9] that the principal axes of rotation in the condensed phase may not correspond to the principal inertial axes through the centre of mass but rather to axes about the centre of volume swept out by the rotating molecule. This involves a coupling of rotation and translation and the value for I_r becomes larger. For the monosubstituted phenyls, the centre of volume is expectedly closer to the ring centre than is the centre of mass so that computing I_r for axes about the former origin gives an upper bound for I_r. Both values of I_r have been used in fitting the data for the chloro-, bromo-, and nitrobenzene solutes, and the alternative fits for chlorobenzene are illustrated in figure 1 (*c*). In figure 1 (*b*) two sets of data [12] for CH_2Cl_2 have been transformed and fitted to indicate the extent of instrumental uncertainty on the derived parameter value. Here curve 1 is the transform of a spectrum averaged from seven different runs, curve 2 is the extremum of this set, caused by a known optical misalignment. Such machine errors inherent in the Michelson instrument are not obvious from the spectra and are only now beginning to be tackled systematically. The (K_0, K_1, γ) set for curve 2 vary by up to 22 per cent of the mean values and this is taken as the maximum possible uncertainty for the results of table 1. Finally we note that for some systems the experimental correlation function is broadened and cannot be simulated very well by (A 11). This is the case for chloroform (figure 1 (*d*)) where induced absorption is likely to contribute, and our simulated curve is consequently chosen to match the region of the minimum rather than the initial cosinal decay.

4.1. *The best-fit parameters of table* 1

The position of the minimum in the rotational velocity autocorrelation function (and therefore β) depends essentially on the spectral band centre position while the depth of the minimum (and α_1) depends on the spectral band width. The former dependency can be confirmed from table 1 by taking the ratio $\beta/\bar{\nu}_{max}$ (with β in unnormalized units) which is then found to be almost constant. This property provides a consistency check for the computed β

values. More significant is the observation that the α_1 values (in unnormalized units) are all within the range $5{\cdot}2 \pm 1{\cdot}4 \times 10^{12}$ s implying a similarity in the band widths of all the spectra studied. This in turn reflects a similarity in the dynamic evolutions of molecules as different as CH_2Cl_2 and 1-bromonaphthalene and is not simply a consequence of using a common solvent. If the spectra (corrected for solvent) are plotted on a normalized scale such as in figure 2 then the small variations in bandshape can be compared. For both extremes of bandshape in this figure (aniline and chloroform solutions) there is a greater uncertainty in spectral measurement. It does appear however that the chloroform and *t*-butylchloride systems are broadened possibly by significant induced absorptions in the high frequency tail, while aniline may be narrow by virtue of there being long range interactions (association) present. The values of α_1 and β may in conclusion be regarded as useful descriptive parameters in comparing far infrared bandshapes.

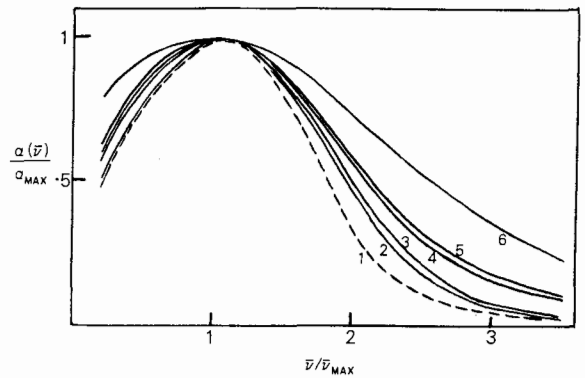

Figure 2. Absorption spectra for solutes in decalin (293 K) on normalized scales: (1) aniline (3·3 ps); (2) CH_2Br_2 (5·4 ps); (3) chlorocyclohexane (3·8 ps); (4) CH_2Cl_2 (6·6 ps); (5) furan (6·5 ps); (6) pyridine (6·4 ps); (7) chloroform (6·5 ps); values in parenthesis are α_1, and reflect spectral width.

The most important parameter from a statistical point of view is the mean square torque $\langle\Gamma(0)^2\rangle$ which can in principle be determined from *a priori* calculation or by computer simulations. This is obtained from (A 5) as $\langle\Gamma(0)^2\rangle = 4kTI_rK_0$ and, at constant T, is therefore proportional to K_0. From table 1 we see that this parameter increases in value with the size of the solute, so supporting our previous rationalization developed [8, 9] between $\langle\Gamma(0)^2\rangle$ and the solute volume of rotation. Actual values of torque are evaluated conconveniently as the root mean square torque per mole.

Next we consider to what extent the statistical parameters of table 1 promote the concept of planar itinerant oscillation as outlined in the Appendix. If I_1 is taken to be larger than $I_2 = I_r$ and if β and ω_0 are given from the observed Debye and librational peak positions, then, as illustrated in figure 3 (*a*) for the pyridine/decalin system (curve 3), the resulting far infrared peak is too

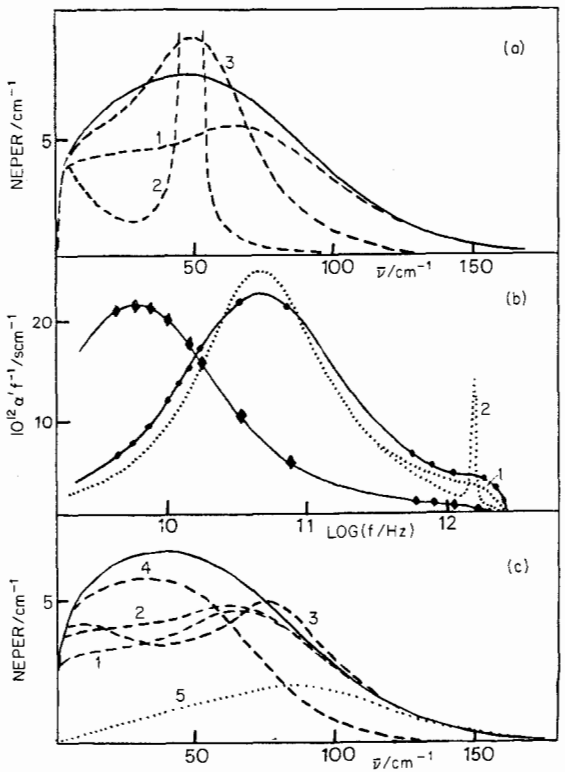

Figure 3. Analytic spectral forms illustrated for two systems of widely differing relaxation times. (*a*) Absorption for pyridine–decalin ($\tau_D = 3{\cdot}1$ ps): ———, experimental; – – – –, analytic fittings. (1) Fit using parameters of table 1 (optional fit at short times); (2) fit using parameters based on itinerant oscillator model ($I_1 > I_2$), ($\bar{K}_0 = 72$, $\bar{K}_1 = 14{\cdot}5$, $\bar{\gamma} = 2{\cdot}9$); (3) intermediate fit ($\bar{K}_0 = 90$, $\bar{K}_1 = 210$, $\bar{\gamma} = 32$). (*b*) 'Loss' spectra; —●—●—●—, experimental data for pyridine–decalin; ……, analytic fits: (1) and (2) as for curves (1) and (2) in figure 3 (*a*); —◆—◆—◆—, experimental data for nitrobenzene–decalin (one-third scale). (*c*) Absorption for nitrobenzene–decalin ($\tau_D = 20$ ps): ——— and – – – –, as figure 3 (*a*). (1), (2) and (3) fits illustrating the effect of α_2 (parameters as in table 2). (4) Fit illustrating the possibility of there being significant induced absorption curve (5), in the observed spectrum.

sharply resonant around $\bar{\nu}_{max}$. The parameters for this and other curves in figure 3 are given in table 2. A more satisfactory, though not perfect, spectral simulation is obtained from the use, in (A 13), of the parameters given in table 1, and is by virtue of the parameters being fully adjustable in the Mori scheme [18]. From the table it is apparent that to reproduce the breadth of the Poley absorption we have to use $\bar{K}_1 > \bar{K}_0$ for all the systems. The equivalence of the parameters (A 12) therefore forces us to the conclusion that the cage moment of

Table 2. The effect of α_2 on spectral fittings (by reference to $PhNO_2$/decalin data, figure 3 (*c*)).

Curve	α_1	α_2	$(I_r/kT)^{1/2} = 1{\cdot}15$ ps β (reduced time units)	$\bar{\gamma}$	$\bar{K}_0$	$\bar{K}_1$	τ_{Mori}/ps
1	8	40	17	56	252	741	22
2	6·7	18	18	31·4	211	398	19
3	4·8	11	18	20·6	185	267	16·4
4	—	—	—	22·6	68	189	12·4

inertia I_1 must be less than that of the encaged dipole, I_2 and so on average contains less than one solvent molecule. This tenuity of the cage points to the following interpretation. The encaging of a dipolar solute is the occasional pairing or clustering of solute with solvent molecules interdispersed with periods of greater rotational freedom. Evidently, we do not have cooperative translation of several molecules fixed in a planar orbit around the solute.

Our next consideration arises from the result that $K_0(0) > (2\pi c\bar{\nu}_{max})^2$ for optimal fitting. This means that the absorption maxima cannot be associated immediately with the root mean square frequency of libration in the molecular ensemble. An explanation however reveals itself through the features of the optimum theoretical absorption spectra as illustrated in figure 3 (*a*) curve 1 for pyridine–decalin. From this example, which is typical, we note that the

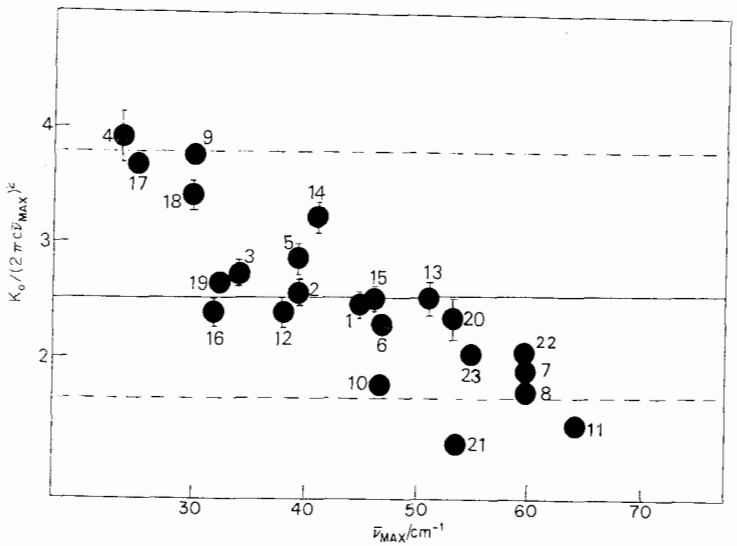

Figure 4. Variation of mean square torque to peak ratio ($K_0/(2\pi c\bar{\nu}_{max})^2$) with peak frequency ($\bar{\nu}_{max}$) for decalin solutions at 293 K. Numbered as in table 1.

curve is twin peaked and underestimates the intensity in the 10–50 cm^{-1} region. Reasons for this failure are given later, but for the present we may interpret the analytical curve, (II), as a band of librational absorption centred at $K_0(0)^{1/2}$, (about 70 cm^{-1}), superimposed on the inertia corrected Debye plateau absorption which gives the lower frequency peak. Clearly these two peaks merge completely in practice giving an observed $2\pi c\tilde{\nu}_{max}$ less than $K_0(0)^{1/2}$ so that the ratios $K_0/(2\pi c\tilde{\nu}_{max})^2$ of table 1 are greater than unity because of the proximity of the Debye process. The ratios for the present systems are grouped around a value of 2·5 and in fact there is a degree of correlation of their values with $\tilde{\nu}_{max}$ (but not with τ_D^{-1}) figure 4. This is not expected from the modelling and is at variance with our relation [8, 9] derived between the peak positions and the solute volumes of rotation, which depends on $K_0/\tilde{\nu}_{max}^2$ being constant. Deviations from this law are therefore useful pointers to the following :

(*a*) the limitations of the Mori/I.O. model, especially when attempts are made to describe zero-THz spectra consisting of widely separated Debye and Poley peak frequencies. In this case K_1/K_0 has to be large, forcing an unnatural narrowness on the theoretical F.I.R. curve. In the extreme of solid-phase libration the Mori/I.O. model cannot be made to produce a broad far infrared curve whilst accounting for the known loss features of the kHz region ;

(*b*) the presence of association, typified by hydrogen-bonding, e.g. aniline and acetone solutions in figure (4) ;

(*c*) the presence of induced absorption [19] in the far infrared.

As the bands of most non-polar systems are centred at comparatively high frequency [2], decalin for example at 70 cm^{-1} and benzene at 80 cm^{-1} it is expected that similar contributions are present in the dipolar bandshapes. If the spectrum of 10 per cent bromobenzene in decalin is corrected by subtraction of a fraction (less than 10 per cent) of the pure benzene spectrum then the

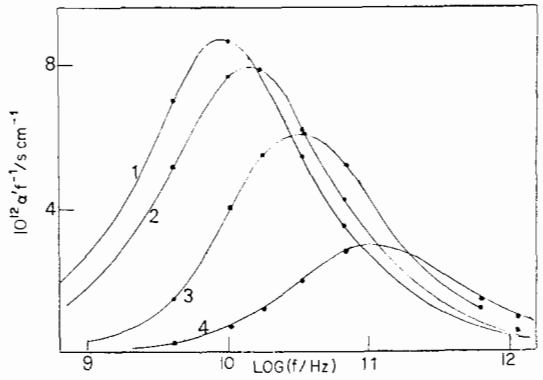

Figure 5. Attentuation/frequency spectra for selected decalin solutions at 293 K. (1) Bromobenzene ; (2) chlorobenzene ; (3) chloroform ; (4) furan.

resulting band is narrower, and the ratio $K_0/(2\pi\tilde{\nu}c)^2$ is smaller. By obtaining more accurate bandshapes (using, for example, a laser source) a plot such as that of figure (4) may be useful for estimating the effects of induced absorption. At present all the points on this figure are within ± 50 per cent of a mean value of 2·5, with the exception of aniline and acetone, which are low.

Our final consideration in this section is that of the accuracy with which the Mori/I.O. model fittings made at short times reproduce the experimental loss data at lower frequencies. For this, the Debye relaxation times of a number of decalin solutions at 293 K (± 2 K) have been obtained by measuring the attenuation coefficients (α') at several microwave frequencies. These determinations, at 4, 10, 18, 37 and 69 GHz are plotted as α'/f in figure 5. For these dilute dipolar systems ($(\epsilon_0 - \epsilon_\infty) < 0{\cdot}4$ except for pyridine, picoline, nitrobenzene and benzonitrile solutions) α'/f is almost identical with the loss and indicates approximate Debye behaviour. The permittivities have been measured statically (ϵ_0) but not at microwave frequencies, where the behaviour is assumed from the shape of the loss curve. If this is to be described, for the sake of argument, by a Debye function then the relation between the observed peak frequency f_{max} of the α'/f curve and the macroscopic relaxation time τ_{exp} is

$$\tau_{exp} = \left[\frac{3\epsilon_0 + \epsilon_\infty}{\epsilon_0 + 3\epsilon_\infty}\right]^{1/2} (2\pi f_{max})^{-1}.$$

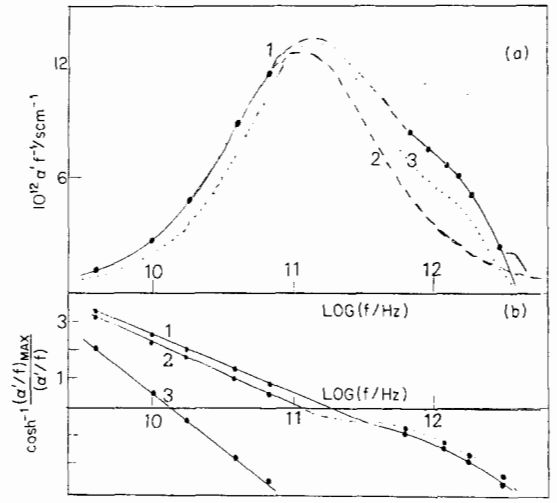

Figure 6. Microwave and far infrared data for CH_2Cl_2–decalin : Fuoss–Kirkwood curves and analytic fits : (*a*) α'/f spectra (approximating dielectric loss) ; ● ● ●, experimental points. (1) Best Fuoss–Kirkwood curve through all data ; (2) Debye curve through low frequency data ; (3) Mori/I.O. analytic best fit (parameters as in table 1). (*b*) Fuoss–Kirkwood plots of curves (1) and (2) above. (3) Plot for chlorobenzene–decalin for comparison.

Table 3. Microwave data for 10 per cent v/v solutes in decalin at 293 K.

Solute	ϵ_0	τ_{exp}/ps		β_{FK}	τ_{lit} (293 ± 5 K)/ps	τ_{Mori}/ps	V^2/Å^6
(1) CH_2Cl_2†	2·59	1·2 ± 0·3	(1·1)	0·9	—	0·95	280
(2) Chloroform†	2·36	4·3 ± 0·3	(4.2)	0·9	3·2cy ; 5·0cl (*a*)	3·1	625
(3) Furan†	2·25	2·0 ± 0·3	(2·0)	0·9	1·9 (*b*)	2·6	678
(4) Pyridine†	2·92	3·4 ± 0·3	(3·1)	0·8	3·1cy ; 4·6b (*b*)	3·35	1263
(5) 2-Methyl-pyridine	2·66	9·0 ± 1	(8·5)	0·7	—	6·5	2724
(6) Tetrahydro-furan†	2·59	2·0 + 0·5	(1·8)	0·9	—		1400
(7) Fluorobenzene	2·47	4·0 ?	(3·9)	0·74	5·4b (*a*) ; 6·8 (*d*)	6·0	2265
(8) Pentafluoro-benzene	2·4	10 ± 1	(9·8)	0·76	—	13·8	3227
(9) Bromobenzene	2·5	16·7 ± 1	(16·2)	0·82	12cl (*a*) ; 14 (*d*)	8·5	5700
						‡16	‡3840
(10) Chlorobenzene	2·46	11·2 ± 1	(10·7)	0·8	8·6cl (*a*) ; 10·2 (*d*)	9·2	3958
						‡12·7	‡3117
(11) (20 per cent) toluene	2·2	9·0 ± 2	(9·0)	—	14cl (*e*)	10·7	4680
(12) (20 per cent) o-xylene	2·27	12 ± 1	(12)	0·8	9cl (*a*)	—	—
(13) Nitrobenzene	4·18	24 ± 3	(20)	0·9	15·2cl (*a*)	13·6	5800
						‡19	‡5020
(14) (5 per cent) benzonitrile	3·0	30 ± 5	(27)	0·7	17cl (*a*) ; 40 (*d*)	12·6	—
(15) 1-Chloro-naphthalene	2·43	30 ± 5	(29)	0·9	18cl (*a*) ; 21 (*f*)	16·6	—
(16) *t*-Butyl-chloride	2·62	3·6 ± 0·3	(3·4)	0·85	3·2cl (*a*)	3·0	1600

† Debye separation arbitrary (see text and figures).
‡ Torque determined inertial axes.
(*a*) to (*e*) = references [20], (*f*) = reference [21].
cy = cyclohexane ; cl = CCl_4 ; b = benzene.

To obtain accurate values of f_{max} a modified Fuoss–Kirkwood equation [17] is used

$$\cosh^{-1}\left[\frac{(\alpha'/f)_{max}}{(\alpha'/f)}\right] = \beta_{FK}\log_e(f_{max}/f).$$

For systems with short relaxation times, the Debye process overlaps with the far infrared absorption and can no longer be found with a Fuoss–Kirkwood plot (figure 6). (The distinction between far infrared and microwave is of course arbitrary.) In this case only the low frequency points can be used to determine τ_{exp}. From the intercepts of these plots with the frequency axis (at f_{max}) experimental relaxation times have been calculated and are shown in table 3, together with β_{FK} parameters and ϵ_0. Some literature solution values [20] are given for comparison in column four but except for 1-chloronaphthalene [21] and chloroform [22] none of the solutes has previously been studied in decalin and no data were found for α-picoline, CH_2Cl_2, tetrahydrofuran or C_6HF_5.

These values are compared with the Mori/I.O. predictions from the far infrared as follows. A field correction was made using the Cole factor [23] (not the Debye–Lorentz field factor) to obtain the molecular τ_D times :

$$\tau_D = \left[\frac{2\epsilon_\infty + \epsilon_0}{3\epsilon_\infty}\right]\tau_{exp}.$$

The values of the experimental τ_D are bracketed in the table and are only significantly smaller for the more polar solutions. The theoretical τ_{Mori} values are nearly all within 30 per cent of the observed values except for fluorobenzene/decalin and C_6HF_5/decalin, which are within 50 per cent, and for solutions of benzonitrile and 1-chloronaphthalene whose long relaxation times are reproduced theoretically to within a factor of two only. For chloro-, bromo- and nitrobenzene solutions the parameters obtained by choosing the larger reduced inertias appropriate to torque-determined axes, give significantly larger and more realistic values of τ_{Mori}. This is further evidence for the ability of zero-THz spectroscopy to investigate roto-translational couplings in detail.

In conclusion, the Mori/I.O. model can be used to simulate both the long and short time details of a large number of solutes in decalin at 293 K and is an improvement over the Wyllie version [24] of itinerant oscillation or the Brot–Larkin model [25], both of which give an unrealistic fast decay (non-cosinal) for $\ddot{C}_\mu(t)$ at short time. The theoretical spectra, however, do not behave satisfactorily in that they are generally twin-peaked and do not merge completely to give the observed single absorption band (figure 5 (*c*)). The region of breakdown of the Mori/I.O. theory can therefore be identified as the intermediate frequency region, 10–80 cm^{-1}. This may be rationalized as follows :

(i) The early approximant used in the model probably does not allow sufficient consideration of the transition from the deterministic (short-time) to stochastic (long-time) regimes.

(ii) There is an unresolved question of the importance of rotation/translation coupling, especially regarding the cooperative nature (cog-wheeling) of large angled motions.

(iii) The onset of dispersive internal-field elements below the 10 cm^{-1} region does not allow us to extend the validity of our autocorrelation function modelling without considering eventually the problem of cross-correlations (e.g. using the theorem of Madden and Kivelson [26]).

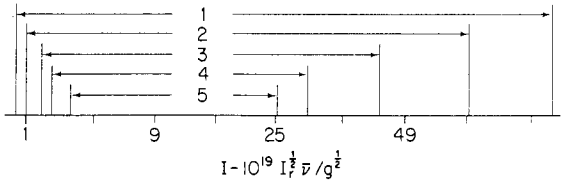

Figure 7. Graph of maxima separations : (1) nitrobenzene ; (2) chlorobenzene ; (3) pyridine ; (4) *t*-butyl chloride ; (5) CH_2Cl_2.

4.2. *Spectral analysis and the problem of collision induced absorption*

We have already briefly considered, in figure 3 (*a*), two spectral simulations of the pyridine–decalin system, both described by (A 13) but each with parameter sets derived from opposing points of view. Curve 1 is based on the parameters given in table 1, and is consequently well representative of the short-time details of the motion (figure 1 (*a*)). This is reflected in figure 3 (*a*) as a correct simulation of the width of the librational profile and its high frequency fall off. The adequacy of the analytic extrapolation to low frequency, already inferred from table 3 where $\tau_{\text{Mori}} \approx \tau_{\text{D}}$, can be seen graphically in figure 3 (*b*) where curve 1 of figure 3 (*a*) is compared with microwave data in the loss representation. Curve 2 of figure 3 (*a*) in contrast illustrates the typical spectral form generated when the parameters are determined from knowledge of the experimental τ_{D} and $\tilde{\nu}_{\max}$ and with the supposition $I_1 > I_2$. This curve can then reproduce the two essential features of the spectrum, the Debye and Poley peaks, in position but not in profile. Clearly neither curve is completely satisfactory in the far infrared and if spectral fitting were divorced from temporal considerations a curve such as 3 in figure 3 (*a*) closely matching the observed peak in position and intensity might be more appropriate. All three curves give identical profiles in the loss representation (figure 3 (*c*)) below about 5 cm^{-1} (150 GHz) which are narrower than those observed. Conversely, as already discussed, the redundancy of α_2 in the temporal curve matching exercises of table 1 makes it necessary to consider a set of curves such as curves 1 to 3 in figure 3 (*c*) in connection with data for nitrobenzene–decalin. Of these three curves, all identical at high frequency or short time, curve 2 is considered to be optimal in this representation and coincidentally also in the loss. The two systems pyridine and nitrobenzene in decalin are extreme in having very different relaxation times of 3·3 ps and 20 ps respectively. Comparison of the fits for each system thus indicates how the I.O. model can reasonably fit the overall spectra (in profile if not intensity) even when the Debye and Poley peaks are well separated in frequency (figure 8). An opposite extreme occurs for dichloromethane in decalin solution where now the loss peaks well above 100 GHz, figure 6 (*a*). An extrapolation, made by fitting both the microwave and far infrared data points on a Fuoss–Kirkwood plot (curve 1 of figure 6 (*b*)) indicates a maximum intensity of greater than $\epsilon''_{\max} = \frac{1}{2}(\epsilon_0 - \epsilon_\infty)$ in this case. This was observed for three other systems (chloroform, tetrahydrofuran and furan) whose losses peak in this region and occurs despite the fact that $\beta_{\text{FK}} < 1$, indicating a broadening of the experimental loss curve. Qualitatively, this is due to a large overlap between the Debye peak and the Poley absorption of the far infrared, and for CH_2Cl_2 the low frequency data does in fact fit on a Debye curve as seen by curves 2 in figures 6 (*a*) and (*b*). The Fuoss–Kirkwood plot for the chlorobenzene/decalin system is also shown for comparison (with its $\cosh^{-1}$ scale doubled) and is typical of data for systems whose losses peak at lower frequency ($\beta_{\text{FK}} = 0{\cdot}7$ to $0{\cdot}9$).

The failure of the Mori/I.O. model to account adequately for the far infrared intensity relates to a similar failure of the Gordon sum rule [27]. It is assumed usually that the additional absorption is due to induced contributions. In table 4 we list the sum rule predictions, A_{G} (corrected by a Polo/Wilson factor for the internal field) against the measured integrated absorptions (A_{exp}) for some of our solutions. The aromatic ring compounds have smaller ratios

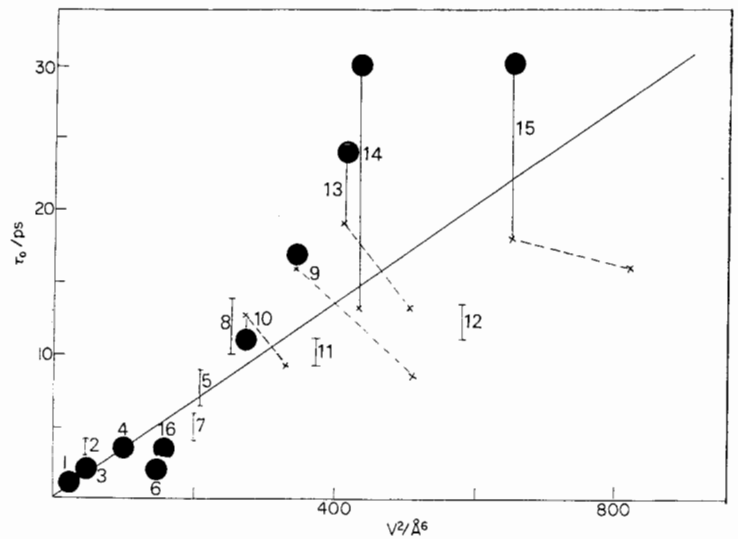

Figure 8. Predicted and observed Debye times and their correlation with V^2 (V = solute volume of rotation). Number as in table 3. X = Mori predictions from far infrared data ● = observed microscopic relaxation times.

Table 4. Experimental and sum rule integrated intensities for decalin systems.

Solute (10 per cent v/v)	A_{exp}/ cm^2	A_{G}/ cm^2	$A_{\text{G}}/A_{\text{exp}}$ (per cent)	Solute	A_{exp}/ cm^2	A_{G}/ cm^2	$A_{\text{G}}/A_{\text{exp}}$ (per cent)
PhF	214	100	47 (47)	2·9 per cent CH_3CN (CCl_4)	1400	1300	93
PhCl	125	76	61 (50)	CH_2Cl_2	1800	1580	88
PhBr	82	47	57 (56)	*t*-Butylchloride	325	266	82 (77)
$PhNO_2$	600	356	59 (58)	2-Chloro-2-nitropropane	571		
5 per cent PhCN	349	231	66 (62)	Chloroform	147	108	73 (88)
Furan	210	95	45	MeI	680		(85)
Pyridine	728			Thiazole	784		
T.H.F.	1300	408	31	Chlorocyclohexane	155		
T.H.P.	293	191	65	2-3-Dihydropyran	273	240	88

$A_{\text{G}}/A_{\text{exp}}$, below 65 per cent compared with those for the saturated molecules and alicyclics. This is notable in the light of the large induced absorption of benzene itself. Tetrahydrofuran is an exception, with an observed absorption over three times that predicted by Gordon, indicating another underlying absorption mechanism (pseudorotation). These ratios for 10 per cent v/v

solutions in decalin are very similar to those obtained for the pure liquids by Hindle *et al.* [28] (bracketed in table 4).

The apparent constancy of the ratio for the halogenobenzenes, despite their different absorption intensities suggests that the induced component in these systems is not simply the same cross-section absorption as for pure benzene. Rather, we assume that it is not wholly due to induced dipoles whose instantaneous directions are random with respect to the present molecular axes but that there is an additional enhancement of the permanent dipole. In other words the instantaneous value of the molecular dipole moment which is responsible for far infrared absorption is larger than the dipole moment observed statically (with an Onsager [29] or Guggenheim [30] equation for example). This could be due to a variety of mechanisms, the following being typical.

(i) According to Debye [31], the solution static permittivity is due to a field orientation of dipoles in counterbalance with thermal rotational diffusion. Each diffusing molecule will appear to contain a dipole of moment μ, but on a shorter time scale the molecules are librating, so the actual dipole μ' (presumed to be at least as large as the gas phase moment) will take a distribution of orientations depending on the mean angle of libration. A calculation shows that if the libration aperture were to be 0·6 rad then the effective moment observed over times larger than the libration period may be 4 per cent smaller than the instantaneous moment.

(ii) The effect of collisions on the dipole may cause its values to fluctuate. Again at longer times a mean value is effective but in the far infrared the absorption intensity depends on the instantaneous value. As Gordon's rule involves μ^2, a random fluctuation of μ about its mean value will give a mean square value larger than the square of the mean. If a dipole of unit mean value is equally likely to take values of 0·7 D and 1·3 D, i.e. a 30 per cent fluctuation, then the mean square dipole is 1·09 D. In addition the effects of dipole–dipole interaction [32] are known to reduce the Onsager determined dipole moment in liquids such as nitrobenzene or benzonitrile compared with μ for an isolated molecule. Assuming that this occurs in most liquid systems (inferred from comparing solution and gas phase dipole moments) then again we must consider a static (Onsager) dipole moment in the dielectric range 0–10 cm^{-1}, and an effective dipole moment, i.e. essentially free of dipole–dipole effects, giving enhanced absorption, in the far infrared.

5. Relating the Poley and Debye absorption peaks

In this section we obtain a simple empirical relation linking these two frequencies. This is useful because their separation on the frequency scale is a direct measure of the mean square torque. It is convenient to normalize the frequency with the square root of the solute reduced inertia. Figure (7) shows the peak separations as a function of molecular geometry. A similar trend is observed with decreasing temperature for a given solute.

The model predictions of τ_D used earlier may be developed to account for the peak separations in a simple empirical way. Comparing the correlation functions $\ddot{C}_\mu(t)$ it becomes clear that the position of the minimum is generally

determined from the spectral peak position, while its depth depends on spectral width. Therefore the unnormalized value of the parameter β is approximately proportional to $\tilde{\nu}_{max}$ for the majority of systems. Further the unnormalized value of α_1 is approximately constant, about $6 \pm 0{\cdot}6$ ps^{-1}, which is an indication of the similarity in bandshape for most of the solute/decalin systems we have studied. Using the approximation $\tilde{\alpha}_1 \ll \tilde{\beta} \approx \tilde{\alpha}_2$ (bars indicate normalization) then $\Gamma \to \tilde{\alpha}_1/\tilde{\beta} \ll 1$ and $\tau_D = (I_r/kT)^{1/2}\,\tilde{\beta}^2/(4\tilde{\alpha}_1)$. Because β is proportional to $\tilde{\nu}_{max}$ and α_1 is constant then $\tau_D \propto (I_r/kT)^{1/2}\,\tilde{\nu}_{max}{}^2$ and consequently the relaxation time is proportional to the square of the solute volume of rotation. These relations assume that the master far infrared bandshape (cf. figure 3) does not vary appreciably from solute to solute.

A similar result may be derived from the Langevin equation for rotational motion. For brownian motion in the absence of a field

$$I\ddot{\theta}(t) = -\zeta\dot{\theta}(t) + \Gamma(t)$$

where ζ is the friction coefficient. The mean square displacement $\langle\theta^2\rangle$ is related to ζ by $\langle\dot{\theta}^2\rangle = 2kTt/\zeta$ and Einstein's result for the diffusion coefficient follows, i.e. $D = kT/\zeta$. The relaxation time τ_D is approximately that for the molecule to have rotated, on average, through an angle of 1·2 rad from its $t = 0$ position, and is proportional to D^{-1}. For planar motion ζ is related to the autocorrelation function of the random torque acting on the molecule,

$$\zeta = (2kT)^{-1} \int_{-\infty}^{\infty} \langle\Gamma(t)\Gamma(0)\rangle\, dt.$$

The basis of the present three variable theory is a generalized Langevin equation where $\zeta\dot{\theta}(t)$ is not independent of previous values of $\dot{\theta}(t)$ and is replaced by $\int_0^t K_0(t-t')\dot{\theta}(t')\,dt'$ where $K_0(t) = \langle\Gamma(t)\Gamma(0)\rangle/2kT$ is the memory function of $\dot{\theta}(t)$. For long time intervals where the rapid fluctuation (libration) of $\dot{\theta}(t)$ is not considered the generalized form reduces to that involving the single friction constant ζ. The random torque correlation function may be decomposed into a solute dependent term V^2 and (to a first approximation) a solute independent term $P(t)$ then we have

$$\tau_D \propto V^2(kT)^{-2} \int_0^{\infty} P(t)\, dt$$

or for a set of solutes in a common solvent at a given T, $\tau_D \propto V^2$, where V is the volume of rotation.

To check the result (which assumes that $P(t)$, the correlation function of torque per unit volume of rotation [8], evolves in a similar manner for all the systems) the experimental τ_D times of table 3 have been plotted against the respective solute volumes V^2 in figure 8. The effect of rotation–translation coupling is shown by dashed lines (i.e. the effect of taking moments of inertia about the centre of volume rather than the centre of mass). The resulting distributions of points appear to be well correlated, although not as well as for the almost linear distribution found between $I_r\tilde{\nu}_{max}{}^2$ and V^2 [8]. This is expected in view of the more complicated (cooperative) behaviour at long times and the consequent dependence of τ_D not only on the far infrared peak position but also on its bandshape. However it seems possible to use a curve such as

that in figure 8 to predict the relative values of τ_D from a simple consideration of solute geometry and to a better accuracy than that predicted by Stokes law :

$$\tau_D = 4\pi a^3 \eta (kT)^{-1},$$

where η is the solvent viscosity.

The Science Research Council is thanked for an equipment grant and a studentship to C.J.R.

Appendix

The Mori representation of the Liouville equation describing the evolution of a random variable $A(t)$, has the form [18, 2]

$$\dot{\mathbf{A}}(t) = i\boldsymbol{\Omega}(t) - \int_0^t K_0(t-\tau)\mathbf{A}(\tau)\, d\tau + \mathbf{R}(t), \tag{A 1}$$

where $\boldsymbol{\Omega}(t)$ is a resonance operator which is null for single molecular motion, $K_0(t)$ is the memory function of $\mathbf{A}(t)$ and $\mathbf{R}(t)$ is the random component of $\dot{\mathbf{A}}(t)$. On multiplying by $\mathbf{A}(0)$ and averaging, equation (A 1) is transformed into

$$\frac{dC_A(t)}{dt} = -\int_0^t K_0(t-\tau)C_A(\tau)\, d\tau \quad \text{where} \quad C_A(t) = \frac{\langle \mathbf{A}(t) \,.\, \mathbf{A}(0)\rangle}{\langle A(0)^2\rangle} \tag{A 2}$$

and has a solution in Laplace space :

$$C_A(p) = 1/(p + K_0(p)). \tag{A 3}$$

The memory function is shown in Mori's work [18] to be itself a correlation function (of the variable $\mathbf{R}(t)$) and may also be described by an equation similar to (A 2) with a second memory function $K_1(t)$. Sequential use of this logic generates a continued fraction expression for $C_A(p)$ which we truncate at first order level by assuming that $K_1(t) = K_1 \exp(-\gamma t)$. With angular velocity $\dot{\theta}(t)$ as the variable, the correlation function expression in Laplace space is now

$$C_{\dot\theta}(p) = \cfrac{1}{p + \cfrac{K_0}{p + \cfrac{K_1}{p+\gamma}}} = \frac{p^2 + \gamma p + K_1}{p^3 + \gamma p^2 + (K_0 + K_1)p + \gamma K_0}. \tag{A 4}$$

As classically, the correlation functions are time-even their Taylor expansions at short times are of the form

$$C_{\dot\theta}(t) = a_0 + \frac{a_1 t^2}{2!} + \frac{a_2 t^4}{4!} + -,$$

and likewise for $K_0(t)$ and $K_1(t)$. Substitution into equation (A 2) and comparing terms gives

$$K_0 = -a_1 = \frac{\langle \ddot\theta(0)^2\rangle}{\langle \dot\theta(0)^2\rangle}; \quad K_1 = a_1 - a_2/a_1 = \frac{\langle \dddot\theta(0)^2\rangle}{\langle \ddot\theta(0)^2\rangle} - \frac{\langle \ddot\theta(0)^2\rangle}{\langle \dot\theta(0)^2\rangle}, \tag{A 5}$$

Transformation of (A 4) generates the angular velocity correlation function in terms of the roots, $-\alpha_1 \pm i\beta$, $-\alpha_2$ of the cubic denominator rather than in terms of K_0, K_1 and γ directly. The two sets of parameters are interrelated by [12] :

$$\gamma = 2\alpha_1 + \alpha_2; \quad K_0 + K_1 = \alpha_1^2 + \beta^2 + 2\alpha_1\alpha_2; \quad \gamma K_2 = (\alpha_1^2 + \beta^2)\alpha_2. \tag{A 6}$$

The orientational correlation function $\langle \mathbf{u}(0) \,.\, \mathbf{u}(t)\rangle$, where $\mathbf{u}$ is the unit dipole vector, must now be derived from the form for $\langle \dot{\boldsymbol{\theta}}(0) \,.\, \dot{\boldsymbol{\theta}}(t)\rangle$, and can only be obtained in closed form for the case of planar reorientation [10]. We have in this case :

$$\langle \mathbf{u}(t) \,.\, \mathbf{u}(0)\rangle = \exp\left\{ -\langle \dot\theta(0)^2\rangle \left(A_1(\exp(-\alpha_1 t)\cos\beta t - 1) - B_1 \exp(-\alpha_1 t)\sin\beta t + \frac{\Gamma}{(1+\Gamma)\alpha_2^2} \,.\, (\exp(-\alpha_2 t) - 1) + C_1 t \right) \right\}, \tag{A 7}$$

where

$$A_1 = \frac{\alpha_1 M + \beta L}{(\alpha_1^2 + \beta^2)(1+\Gamma)}, \quad B_1 = \frac{\beta M - \alpha_1 L}{(\alpha_1^2 + \beta^2)(1+\Gamma)}, \quad C_1 = \frac{(M + \Gamma/\alpha_2)}{(1+\Gamma)},$$

$$M = \frac{2\alpha_1 + \alpha_2\Gamma}{\alpha_1^2 + \beta^2}, \qquad L = \frac{\alpha_1 M - 1}{\beta}, \qquad \Gamma = \frac{2\alpha_1(\alpha_1^2 + \beta^2)}{\alpha_2(\beta^2 + \alpha_2^2 - 3\alpha_1^2)}.$$

The mean square angular velocity, $\langle \dot\theta(0)^2\rangle$ is kT/I in this case. For a spherical top having the same moment of inertia I as for the disc, the form for $\langle \mathbf{u}(t) \,.\, \mathbf{u}(0)\rangle$ [10] is essentially identical to equation (A 7) but with $\langle \dot\theta(0)^2\rangle = 2kT/I$. It would then appear that equation (A 7) could be generalized to apply to spatial rotation of asymmetric tops by using the result [13] $\langle \dot\theta(0)^2\rangle = kT/I_r$ where I_r is the reduced inertia

$$I_r = (u_b^2 + u_c^2)I_a^{-1} + (u_c^2 + u_a^2)I_b^{-1} + (u_a^2 + u_b^2)I_c^{-1}. \tag{A 8}$$

A similar argument may be applied to $\langle \ddot\theta(0)^2\rangle$ in (A 5) to reveal the mean square torque $\langle \Gamma(0)^2\rangle = 4I_r^2\langle \dot\theta(0)^2\rangle$ and hence the useful result

$$\langle \Gamma(0)^2\rangle = 4kTI_rK_0. \tag{A 9}$$

At long times, (A 7) becomes purely empirical with a relaxation time the inverse of $(kT/I_r)C_1$. Algebraic manipulation shows that C_1 can be simplified to $K_1/(\gamma K_0)$, which is the zeroth power term in (A 4). We thus have an important result

$$\tau_{\text{Mori}} = (I_r/kT) \,.\, \gamma K_0/K_1. \tag{A 10}$$

More relevant to far infrared behaviour is the rotational velocity correlation function [15] which is the direct Fourier transform of the absorption spectrum, and is given analytically as (minus) the second derivative of (A 7). To simplify this function it is useful to work in reduced units of $(kT/I_r)^{1/2}$. Denoting reduced time by $\hat{t}$ we have [12] :

$$\frac{\langle \dot{\mathbf{u}}(\hat{t}) \,.\, \dot{\mathbf{u}}(0)\rangle}{\langle \dot{\mathbf{u}}(\hat{t}) \,.\, \dot{\mathbf{u}}(0)\rangle} = (\cos\beta\hat{t} + (\beta M + \alpha_1 L)\sin\beta\hat{t})\exp(-\alpha_1\hat{t})/(1+\Gamma) + \Gamma\exp(-\alpha_2\hat{t})/(1+\Gamma) - (1+\Gamma)^{-2} \times \{[L\sin\beta\hat{t} + M\cos\beta\hat{t}]\exp(-\alpha_1\hat{t}) + (\Gamma/\alpha_2)(\exp(-\alpha_2\hat{t}) - 1) - M\}^2, \tag{A 11}$$

where now all coefficients are reduced (but not barred for clarity). The parameters K_0, K_1 and γ derived from the coefficients, in (A 6) are denoted by $\bar{K}_0$, $\bar{K}_1$, $\bar{\gamma}$.

The phenomenological model of itinerant oscillation described and analysed by Calderwood and Coffey [11] consists of a central disc of moment of inertia I_2 harmonically bound to an annulus of inertia I_1 the latter undergoing brownian rotation through the influence of the surroundings. The characteristic frequency of the disc librating within the annulus is ω_0, the motion giving rise to resonant absorption in the far infrared. The brownian rotation gives rise to relaxational behaviour with a characteristic time (τ) determined by the friction coefficient $\beta' = (kT/I_1)\tau$. In applying this model to liquid systems I_2 is identified (in this article) with the solute reduced-inertia. On intuitive grounds ω_0 is identified with $2\pi c\bar{\nu}_{\max}$, the far infrared peak position, I_1 is adjustable but larger than I_2, and β is determined from the observed Debye time. Solution of the equations of motion for this system lead [11, 6] to equations identical in form to (A 4), (A 7) and (A 11), with the substitutions :

$$K_0 \to \omega_0^2 ; \quad K_1 \to \Omega_0^2 = I_2\omega_0^2/I_1 ; \quad \gamma \to \beta'. \tag{A 12}$$

The equations evolved from the Mori approximant or the itinerant oscillator theories are thus equivalent although the two approaches are distinct but complementary.

The form for the analytic spectrum may best be derived in the manner of Calderwood and Coffey [11] via the complex polarizability :

$$\frac{\alpha_\mu(s)}{\alpha_\mu(0)} = \frac{kT}{I_2} \cdot \frac{s^2 + \beta' s + \Omega_0^2}{(s^3 + \beta' s^2 + (\omega_0^2 + \Omega_0^2)s + \beta'\omega_0^2)(s + K_2)}$$

where

$$s = i\omega \quad \text{and} \quad K_2 = \frac{kT}{I_2}\frac{\Omega_0^2}{\beta'\omega_0^2}.$$

We have, in this work, derived the expression for the absorption spectrum to obtain [12] (in terms of the Mori parameters) :

$$n(\omega)\alpha(\omega) = (kT/I_r)(\epsilon_0 - \epsilon_\infty)\omega/c \,.\, (\omega\gamma A - B(K_1 - \omega^2)(A^2 + B^2)^{-1}, \tag{A 13}$$

where

$$A = \omega^4 - \omega^2(K_0 + K_1 + K_2\gamma) + K_2\gamma K_0, \quad B = \omega(\gamma(K_0 - \omega^2) + K_2(K_0 + K_1 - \omega^2))$$

and $n(\omega)$, the refractive index is almost constant in the far infrared region for the dilute solutions studied.

References

[1] Evans, G. J., and Evans, M. W., 1976, *J. chem. Soc., Faraday Trans. II*, **72,** 1169. Evans, G. J., and Evans, M. W., 1978, *J. Chim. phys.*, **75,** 523.
[2] Evans, M. W., 1977, *Adv. Molec. Rel. Int. Proc.*, **10,** 203.
[3] Reid, C. J., Yadav, R. A., Evans, G. J., Davies, G. J., and Evans, M. W., 1978, *J. chem. Soc. Faraday Trans. II*, **74,** 2143.
[4] Nee, T. W., and Zwanzig, R., 1970, *J. chem. Phys.*, **52,** 6353.
[5] Evans, M. W., 1975, *J. chem. Soc., Faraday Trans. II*, **71,** 2051.

[6] Coffey, W. T., Evans, G. J., Evans, M. W., and Wegdam, G. H., 1978, *J. chem. Soc., Faraday Trans. II*, **74,** 310. Coffey, W. T., and Evans, M. W., 1978, *Molec. Phys.*, **35,** 975.
[7] Coffey, W. T., Evans, M. W., and Evans, G. J., 1979, *Molec. Phys.*, **38,** 477.
[8] Reid, C. J., 1979, *Chem. Phys. Lett.*, **66,** 517.
[9] Reid, C. J., and Evans, M. W., 1980, *J. chem. Soc., Faraday Trans. II* **76,** 286.
[10] Evans, M. W., 1977, *Molec. Phys.*, **34,** 963 ; 1976, *Chem. Phys. Lett.*, **39,** 601.
[11] Calderwood, J. H., and Coffey, W. T., 1977, *Proc. R. Soc.* A, **356,** 269.
[12] Reid, C. J., 1979, Thesis, Univ. of Wales.
[13] Brot, G., 1975, *J. chem. Soc., Diel. Rel. Molec. Proc.*, **2,** 1.
[14] Reid, C. J., Evans, G. J., and Evans, M. W., 1978, *Chem. Phys. Lett.*, **56,** 529. Reid, C. J., and Evans, M. W., 1979, *J. chem. Soc., Faraday Trans. II* **75,** 1213.
[15] Gerschel, A., Darmon, I., and Brot, C., 1972, *Molec. Phys.*, **23,** 317.
[16] Chamberlain, J., 1979 (completed by Chantry, G., and Stone, N. W. B.), *The Principles of Interferometric Spectroscopy* (Wiley).
[17] Price, A. H., and Wegdam, G. H., 1977, *J. Phys.* E, **10,** 478.
[18] Mori, H., 1965, *Prog. theor. Phys.*, **33,** 423 ; 1966, *Ibid.*, **34,** 399.
[19] Evans, M., 1975, *Molec. Phys.*, **29,** 1345.
[20] (a) 1957, *Circ. U.S. natn. Bur. Stand.*, No. 501. (b) Crossley, J., and Hassel, W., 1969, *Can. J. Chem.*, **46,** 218. (c) 1970, *Dielectrics*, p. 29. (d) Tucker, S., and Walker, S., 1966, *Trans. Faraday Soc.*, **62,** 2690. (e) Hassel, W., and Walker, S., 1966, *Trans. Faraday Soc.*, **62,** 861.
[21] Grubb, E., and Smyth, C. P., 1961, *J. Am. chem. Soc.*, **83,** 4122.
[22] Meakins, R. J., 1958, *Trans. Faraday Soc.*, **54,** 1160.
[23] Glarum, S. H., 1960, *J. chem. Phys.*, **33,** 1371.
[24] Wyllie, G., 1971, *J. Phys.* C, **4,** 564.
[25] Hoffmans, R., and Larkin, I., 1972, *J. chem. Soc., Faraday Trans.*, **68,** 1729. Larkin, I. W., 1972, *Faraday Symp.*, **6,** 112.
[26] Kivelson, D., and Madden, P., 1975, *Molec. Phys.*, **30,** 1749.
[27] Gordon, R. G., 1965, *J. chem. Phys.*, **43,** 1307.
[28] Hindle, P., Walker, S., and Warren, J., 1975, *J. chem. Phys.*, **62,** 3230.
[29] Onsager, L., 1936, *J. Am. chem. Soc.*, **58,** 1486.
[30] Davies, M., 1979, *Organic Liquids*, edited by A. D. Buckingham (Academic Press, Eurochem. Conference), p. 169.
[31] Debye, P., 1912, *Phys. Z.*, **13,** 97.
[32] Kielich, S., and Piekara, A., 1959, *Acta phys. pol.*, **18,** 439.